Fertigation in furrows and level furrow systems I: model description and numerical tests

J. Burguete[1], N. Zapata[2], P. García-Navarro[3], M. Maïkaka[4], E. Playán[5], and J. Murillo[6]

[1]: *Researcher, Dept. Suelo y Agua, Estación Experimental de Aula Dei, CSIC. P.O. Box. 202, 50080 Zaragoza, Spain. E-mail: jburguete@eead.csic.es*

[2]: *Researcher, Dept. Suelo y Agua, Estación Experimental de Aula Dei, CSIC. P.O. Box. 202, 50080 Zaragoza, Spain. E-mail: vzapata@eead.csic.es*

[3]: *Professor, Dept. Fluid Mechanics, Centro Politécnico Superior, University of Zaragoza. María de Luna 3, 50018 Zaragoza, Spain. E-mail: pigar@unizar.es*

[4]: *Engineering, SERS Consulting, Paseo Rosales 34, 50008 Zaragoza. Spain. E-mail: TIEMAGO@terra.es*

[5]: *Researcher, Dept. Suelo y Agua, Estación Experimental de Aula Dei, CSIC. P.O. Box. 202, 50080 Zaragoza, Spain. E-mail: playan@eead.csic.es*

[6]: *Assistant Professor, Dept. Fluid Mechanics, Centro Politécnico Superior, University of Zaragoza. María de Luna 3, 50018 Zaragoza, Spain. E-mail: Javier.Murillo@unizar.es*

Abstract

The simulation of fertigation in furrows and level furrow systems faces a number of problems resulting in relevant restrictions to its widespread application. In this paper, a simulation model is proposed that addresses some of these problems by: 1) implementing an infiltration model that adjusts to the variations in wetted perimeter; 2) using a friction model that adjusts to different flows and which uses an absolute roughness parameter; 3) adopting an equation for the estimation of the longitudinal diffusion coefficient; and 4) implementing a second order TVD numerical scheme and specific treatments for the boundary conditions and the junctions. The properties of the proposed model were demonstrated using three

numerical tests focusing on the numerical scheme and the treatments. The application of the model to the simulation of furrows and furrow systems is presented in a companion paper, in which the usefulness of the innovative aspects of the proposed model is demonstrated.

Keywords: Infiltration, Furrow irrigation, Surface irrigation, Shallow water, Flow simulation, Numerical models.

INTRODUCTION

The numerical simulation of hydrodynamics is a common technique for irrigation analysis, from conveyance networks to on-farm systems. Surface irrigation systems are characterized by their operational simplicity and their complicated analysis and design. The numerical analysis of surface irrigation systems started in the 1970s, aiming at optimizing design and management by maximizing the insight obtained from resource consuming field experiments. Furrow fertigation is a popular surface irrigation system, characterized by one-dimensional flow and wetted perimeter dependent infiltration.

Fertigation (the application of fertilizers dissolved in irrigation water) is a common agricultural technique. It is not only agronomically suited to many crops, but it also constitutes the preferred technical solution to the fertilization of field crops developing tall canopies. For these cases, fertigation is much easier to implement and manage in sprinkler irrigation than in surface irrigation. However, surface irrigation farmers resort to fertigation for a number of crops and in a number of areas of the world. In fact, surface fertigation can result in a reduction of labour, energy, use of machinery and soil compaction as compared to the conventional application of fertilizers.

It was not until the end of the twentieth century that basin and border fertigation was addressed through experimentation and numerical analysis (Boldt et al. 1994; Playán and Faci 1997). These authors applied advective models to the results of surface irrigation simulation and to the identification of optimum fertilizer application practices. Field experiments permitted to explore the conditions of irrigation performance and fertilizer application resulting in adequate estimations of fertilizer distribution uniformity and application efficiency.

García-Navarro et al. (2000) presented a hydrodynamic model of basin and border fertigation, using a McCormack numerical scheme. The model was calibrated and validated using experiments on pervious and impervious borders. Impervious experiments were designed to eliminate the uncertainties derived from infiltration estimation. A diffusion coefficient was introduced in the formulation and estimated via calibration to experimental results. Solute transport in furrows represents an additional challenge due to the complexity of furrow infiltration. Abbasi et al. (2003a) reported the results of a detailed experiment revealing the 2D features of furrow fertigation in what refers to water and solute infiltration. Abbasi et al. (2003b) presented a Crank-Nicholson fertigation model including a routine for the estimation of the diffusion coefficient using a model initially derived for solute transport in soils (Bear 1972). Sabillón and Merkley (2004) presented an advective implicit model simulating furrow fertigation, and identified guidelines for optimum fertilizer application. A split-operator hydrodynamic simulation model for border and basin fertigation was proposed and evaluated by Zerihun et al. (2005a, 2005b), using the same approach for the diffusion coefficient proposed by Bear (1972). These authors coupled overland hydraulics to the HYDRUS-1D model (Simunek et al. 1998) for subsurface flow, and reported adequate agreement between observed and simulated solute distribution. Adamsen et al. (2005) reported a series of field experiments using bromide as a tracer. These authors identified strategies aiming at developing fertigation rules for their experimental conditions. Finally, Strelkoff et al. (2006) reported the extension of the surface irrigation model SRFR to simulate fertigation using an advective scheme.

The review of the literature shows that furrow irrigation has been simulated using a variety of approaches, with the hydrodynamic approach being the most common now a days. Following this approach, the well-known Saint Venant equations are typically solved in combination with two additional empirical equations representing the physical processes of roughness and infiltration. The characterization of roughness requires estimation of the Gauckler-Manning number, a parameter which is often described as dependent on soil surface

conditions, but which also depends on the irrigation discharge. Infiltration estimation is not an easy task even in flat geometry surface irrigation systems such as borders and basins. Numerical parameter estimation techniques have often been applied to this problem, and the resulting parameters only represent the soil surface in the particular experimental conditions. In furrow irrigation systems, infiltration additionally depends on furrow geometry and on wetted perimeter, therefore increasing the number of model parameters and making the use of models a more complicated task. Characterizing furrow infiltration therefore stands as a relevant obstacle to simulation. Although the complexity of furrow infiltration has been analysed and modelled using a number of approaches (Walker and Skogerboe 1987), practical applications have not been abundant due to the requirements on experimental data. When it comes to simulating the transport of neutrally buoyant solutes, furrow models fluctuate between the simplicity of the advective models and the complexity of advective-diffusive models. This complexity is not restricted to the programming effort, but also extends to the identification of the longitudinal diffusion coefficient. Even when predictive equations have been used to estimate the diffusion coefficient, the sensitivity of model results to this parameter has often been analysed in an attempt to derive better parameter estimates.

The analysis of previous efforts suggests that three aspects of furrow fertigation simulation seem to require further attention: infiltration, roughness and fertilizer dispersion. Furrow fertigation is an active field of research in which simplified advective models are used because of the difficulties related to introducing additional simulation parameters and performing additional computations. While this may be an adequate choice in many cases, particular furrow configurations and experimental conditions require an adequate treatment of fertilizer hydrodynamic dispersion. There is a need for numerical models of furrow fertigation using a few, physically based parameters which can be either measured or estimated from experimental measures.

In the last decades, a particular type of furrow irrigation systems has become very popular among farmers in certain areas of the world: level furrows (Walker and Skogerboe 1987). In

this system, a zero-slope field with one inflow point is furrowed at the beginning of the season. Water builds up at the upstream distribution channel as it starts flowing down the irrigation furrows and recirculating through the downstream distribution channel once water advances to the downstream end of some irrigation furrows (Playán et al. 2004). Level furrows are characterized by requiring very little labour and by a high potential application efficiency. Irrigation simulation in level furrow systems was reported by García-Navarro et al. (2004).

In this work, a coupled model of water flow and solute transport is presented for the simulation of surface fertigation in furrows and level furrow systems. Particular attention is paid to the following aspects:

- the infiltration model in furrow geometry, incorporating the model proposed by Maïkaka (2004);
- the friction term, implementing the recent developments by Burguete et al. (2007c) aiming at introducing an absolute roughness parameter;
- the model proposed by Rutherford (1994) to describe the chemical diffusion coefficient; and
- the numerical techniques used for the solution of the governing set of equations.

An experimental field study was specifically designed to validate the proposed model and is presented in a companion paper, together with additional model applications.

GOVERNING EQUATIONS

Shallow-water model

The one-dimensional system formed by the cross sectional averaged liquid and solute mass conservation, momentum balance in main stream direction, infiltration and solute transport can be expressed in conservative form as:

$$\frac{\partial \mathbf{U}}{\partial t} + \frac{\partial \mathbf{F}}{\partial x} = \mathbf{I} + \mathbf{S}^c + \frac{\partial \mathbf{D}}{\partial x} \tag{1}$$

where $\mathbf{U}$ is the vector of conserved variables, $\mathbf{F}$ the flux vector, $\mathbf{S}^c$ the source term vector, $\mathbf{I}$ the infiltration vector and $\mathbf{D}$ stands for diffusion:

$$\mathbf{U} = \begin{pmatrix} A \\ Q \\ As \end{pmatrix}, \quad \mathbf{F} = \begin{pmatrix} Q \\ gI_1 + \frac{Q^2}{A} \\ Qs \end{pmatrix}, \quad \mathbf{S}^c = \begin{pmatrix} 0 \\ g[I_2 + A(S_0 - S_f)] \\ 0 \end{pmatrix}, \quad \mathbf{I} = \begin{pmatrix} -Pi \\ 0 \\ -Pis \end{pmatrix},$$

$$\mathbf{D} = \begin{pmatrix} 0 \\ 0 \\ K_x A \frac{\partial s}{\partial x} \end{pmatrix} \tag{2}$$

with A the wetted cross sectional area, Q the discharge, s the cross sectional average solute concentration, g the gravity constant, S_0 the longitudinal bottom slope, S_f the longitudinal friction slope, K_x the diffusion coefficient, i the infiltration rate, P the cross sectional wetted perimeter. I_1 and I_2 represent pressure forces:

$$I_1 = \int_0^H (H - z'')w \, dz'', \quad I_2 = \int_0^H (H - z'')\frac{\partial w}{\partial x} \, dz'' \tag{3}$$

with H the water depth and w the cross section width (see Figure 1 for the system of reference). The furrows are modellled as pervious prismatic channels of trapezoidal cross section as represented in Figure 2. In this case, the pressure integrals become:

$$I_1 = \frac{B_0 H^2}{2} + \frac{SH^3}{3}, \quad I_2 = 0 \tag{4}$$

with B_0 the base width and S the tangent of the angle between the furrow walls and the vertical direction. The set of equations is completed with the laws for infiltrated volume of water and solute:

$$\frac{\partial \alpha}{\partial t} = Pi, \quad \frac{\partial \phi}{\partial t} = Pis \tag{5}$$

with α the volume of water infiltrated per unit length of furrow and ϕ the mass of solute infiltrated per unit length of the furrow.

The system of equations (1) can be expressed in non-conservative form taking into account:

$$\frac{d\mathbf{F}(x,\mathbf{U})}{dx} = \frac{\partial \mathbf{F}}{\partial x} + \mathbf{J}\frac{\partial \mathbf{U}}{\partial x}, \quad \mathbf{J} = \frac{\partial \mathbf{F}}{\partial \mathbf{U}} = \begin{pmatrix} 0 & 1 & 0 \\ c^2 - u^2 & 2u & 0 \\ -us & s & u \end{pmatrix} \tag{6}$$

where $\mathbf{J}$ is the flux Jacobian, $u = \frac{Q}{A}$ is the cross sectional average velocity, $c = \sqrt{\frac{gA}{B}}$ is the velocity of the infinitesimal waves and B is the cross section top width. Inserting in (1):

$$\frac{\partial \mathbf{U}}{\partial t} + \mathbf{J}\frac{\partial \mathbf{U}}{\partial x} = \mathbf{I} + \mathbf{S}^{nc} + \frac{\partial \mathbf{D}}{\partial x} \tag{7}$$

with $\mathbf{S}^{nc}$ the non-conservative source term:

$$\mathbf{S}^{nc} = \mathbf{S}^{c} - \frac{\partial \mathbf{F}}{\partial x} = \begin{pmatrix} 0 \\ c^2 \frac{\partial A}{\partial x} - gA\left(\frac{\partial z_s}{\partial x} + S_f\right) \\ 0 \end{pmatrix} \tag{8}$$

where z_s is the water surface level. The Jacobian matrix can be made diagonal:

$$\mathbf{J} = \mathbf{P}\mathbf{\Lambda}\mathbf{P}^{-1}, \quad \mathbf{P} = \begin{pmatrix} 1 & 1 & 0 \\ \lambda_1 & \lambda_2 & 0 \\ s & s & 1 \end{pmatrix}, \quad \mathbf{\Lambda} = \begin{pmatrix} \lambda_1 & 0 & 0 \\ 0 & \lambda_2 & 0 \\ 0 & 0 & \lambda_3 \end{pmatrix} \tag{9}$$

with $\mathbf{\Lambda}$ the eigenvalues diagonal matrix, $\mathbf{P}$ the diagonalizer matrix and λ_i the Jacobian eigenvalues corresponding to the propagation characteristic celerities:

$$\lambda_1 = u + c, \quad \lambda_2 = u - c, \quad \lambda_3 = u \tag{10}$$

Furrow infiltration model

One of the most widely used empirical models in surface irrigation is the Kostiakov model relating the infiltration depth Z to the opportunity time τ:

$$Z = K\tau^a \tag{11}$$

where K is the Kostiakov constant and a is the Kostiakov exponent, both empirical parameters depend on soil type, soil water and compactation. From (11), the expression for the infiltration rate can be derived:

$$i = \frac{dZ}{dt} = Ka\tau^{a-1} \tag{12}$$

Working out τ from (11) and inserting it in (12) it can be re-expressed in terms of the infiltration depth (Maïkaka 2004):

$$i = Ka\left(\frac{Z}{K}\right)^{\frac{a-1}{a}} \tag{13}$$

For long infiltration events, the Kostiakov model does not predict the correct infiltration rate. In these cases, it is necessary to introduce the saturated infiltration long-term rate i_c (Walker and Skogerboe 1987). Then, the Kostiakov-Lewis model is obtained:

$$i = i_c + Ka\tau^{a-1} \approx i_c + Ka\left(\frac{Z}{K}\right)^{\frac{a-1}{a}} \tag{14}$$

In furrows, the amount of water infiltrated per unit time and furrow length is proportional to the wetted perimeter. Therefore, using opportunity time as the only independent variable in furrow infiltration such as in (11) or (12) is not correct, since infiltration will depend not only on the time during which water has been infiltrating but also on the surface water present in the furrow itself. Some authors (Playán et al. 2004) tried to modify expression (11) by introducing a dependence on the discharge, however, the results obtained with that model are contradictory in cases of transient inlet discharge. We believe that (13) can be

actually much more representative of the real event since it contains the dependence of i on Z, including the effects of opportunity time and the time evolution of wetted perimeter.

Our aim is to be able to move from (14) to an equivalent form valid in furrows trying to preserve the dimensionality and physical meaning of the Kostiakov-Lewis parameters. For that purpose, Z will be replaced by α divided by the furrow spacing D so that, in furrows:

$$i = i_c + Ka\left(\frac{\alpha}{DK}\right)^{\frac{a-1}{a}} \tag{15}$$

and this infiltration rate will be considered uniform all along the wetted perimeter P, in a form that permits to model the time variation of infiltrated area as (Maïkaka 2004):

$$\frac{d\alpha}{dt} = Pi = P\left[i_c + Ka\left(\frac{\alpha}{DK}\right)^{\frac{a-1}{a}}\right], \quad \frac{d\phi}{dt} = s\frac{d\alpha}{dt} = sP\left[i_c + Ka\left(\frac{\alpha}{DK}\right)^{\frac{a-1}{a}}\right] \tag{16}$$

Friction model

The friction slope is widely modelled by means of the Gauckler-Manning law (Gauckler 1867; Manning 1890):

$$S_f = \frac{n^2 Q|Q|P^{4/3}}{A^{10/3}} \tag{17}$$

For a furrow of trapezoidal cross section:

$$S_f = \frac{n^2 Q|Q|\left(B_0 + 2H\sqrt{1+S^2}\right)^{4/3}}{(B_0 + 2SH)^{10/3}} \tag{18}$$

A more recent model (Burguete et al. 2007c), that showed a better performance in cases of high relative roughness, assumes that the velocity profile can be fit by means of a power function in the roughness upper zone, being negligible in the lower zone:

$$v_x = u_l\left(\frac{z - z_b - z'}{l}\right)^b, \text{ if } z \geq l + z_b + z' \tag{19}$$

where b is a fitting exponent and u_l is the water velocity at a vertical distance l of the

bed. This model also assumes that the bed roughness irregularities are of average size l. Neglecting the lateral exchanges of momentum, the velocity distribution that minimizes the friction energy losses can be obtained (Burguete et al. 2007c; Burguete et al. 2007a):

$$S_f = \frac{|Q|Q}{g\left[\int \frac{1}{(b+1)\sqrt{\epsilon}}\left(\frac{h^{b+(3/2)}}{l^b} - l\sqrt{h}\right)\,dy\right]^2} =$$

$$= \frac{\epsilon(b+1)^2 l^{2b}|Q|Q}{g\left\{B_0\left(H^{b+(3/2)} - \sqrt{H}l^{1+b}\right) + 2S\left[\frac{H^{b+(5/2)}-l^{b+(5/2)}}{b+(5/2)} - \frac{2}{3}l^{1+b}\left(H^{3/2}-l^{3/2}\right)\right]\right\}^2} \qquad (20)$$

where ϵ is a dimensionless parameter of aerodynamical resistance depending only, in turbulent flows, on the roughness shape. This friction law is only valid for $H > l$. If $H < l$ a zero velocity condition is imposed for numerical stabilization of the advance over a dry bed. Figure 3 shows a comparison of the friction slopes estimated by the Gauckler-Manning and the proposed model for a typical furrow assuming a uniform flow velocity. The predicted values are similar for high water depth values. However, the proposed model provides higher values than the Manning model for low water depths.

Solute dispersion model

The diffusion coefficient contains all the information related to molecular or viscous diffusion, turbulent diffusion and dispersion derived from the averaging process. The model proposed by Rutherford (1994) will be used for practical applications:

$$K_x = 10\sqrt{gPA|S_f|} \qquad (21)$$

NUMERICAL MODEL

The numerical scheme used in this paper is based on a previous study developed to demonstrate its suitability for the coupled simulation of the flux and transport equations (Burguete et al. 2007b). In order to incorporate the infiltration process to these equations, a four step algorithm is applied:

1. In the first step, the flow equations and the advective part of the transport equation are discretized with the explicit scheme, and the diffusion term is discretized implicitly:

$$\mathbf{U}_i^a = \mathbf{U}_i^n + \Delta t \left[\left(\mathbf{S}^c - \frac{\partial \mathbf{F}}{\partial x} \right)_i^n + \left(\frac{\partial \mathbf{D}}{\partial x} \right)_i^a \right] \tag{22}$$

2. In a second step infiltration is discretized as follows:

$$\mathbf{U}_i^b = \mathbf{U}_i^a + \Delta t \mathbf{I}_i^a \tag{23}$$

3. In a third step, the source terms are added with an implicit discretization:

$$\mathbf{U}_i^c = \mathbf{U}_i^b + \theta \Delta t (\mathbf{S}_i^c - \mathbf{S}_i^b) \tag{24}$$

where $\theta \in [0, 1]$ is the parameter controlling the degree of implicitness of the source term. We shall use $\theta = 0.5$ in all model runs.

4. Finally, the boundary conditions are applied at the inlet, outlet and furrow confluences (characteristic of level furrow systems) to obtain the conserved variable in the next step $\mathbf{U}_i^{n+1}$.

First step: flow and transport

This part is based on defining the vectors at the cell interfaces:

$$\mathbf{G}_{i+(1/2)}^n = \left(\mathbf{S}^c - \frac{\delta \mathbf{F}}{\delta x} \right)_{i+(1/2)}^n \tag{25}$$

using the notation $\delta f_{i+(1/2)} = f_{i+1} - f_i$ and $f_{i+(1/2)} = (f_{i+1} + f_i)/2$. It is important to note that in the part of the source term corresponding to the friction term, a numerical limitation

of the friction source term is performed (Burguete et al. 2007a):

$$(gAS_f)^n_{i+(1/2)} = \min\left[\frac{(gAS_f)^n_{i+1}+(gAS_f)^n_i}{2},\ \frac{Q^n_{i+(1/2)}}{\Delta t} - \frac{\delta}{\delta x}\left(\frac{Q^2}{A}\right)^n_{i+(1/2)} - \left(gA\frac{\delta z_s}{\delta x}\right)^n_{i+(1/2)}\right] \tag{26}$$

Then, the numerical scheme is built by defining the upwind vectors as:

$$\mathbf{G}^{\pm} = \frac{1}{2}[\mathbf{1} \pm \mathbf{P}\text{sign}(\mathbf{\Lambda})\mathbf{P}^{-1}]\mathbf{G}, \quad \mathbf{\Lambda}^{\pm} = \frac{1}{2}(\mathbf{\Lambda} \pm |\mathbf{\Lambda}|) \tag{27}$$

where the matrices $\mathbf{P}$ and $\mathbf{\Lambda}$ are based on Roe's averages:

$$\lambda_{i+(1/2)} = \frac{\sqrt{A_{i+1}}\lambda_{i+1}+\sqrt{A_i}\lambda_i}{\sqrt{A_{i+1}}+\sqrt{A_i}}, \quad s_{i+(1/2)} = \frac{\sqrt{A_{i+1}}s_{i+1}+\sqrt{A_i}s_i}{\sqrt{A_{i+1}}+\sqrt{A_i}} \tag{28}$$

The artificial viscosity coefficient defined is as (Burguete and García-Navarro 2004):

$$\nu^n_{i+(1/2)} = \max_k \begin{cases} \frac{1}{4}\left[\delta(\lambda_k) - 2|\lambda_k|\right]^n_{i+(1/2)}, & \text{if } (\lambda_k)^n_i < 0 \text{ and } (\lambda_k)^n_{i+1} > 0 \\ 0, & \text{otherwise} \end{cases} \tag{29}$$

the second order vectors as:

$$\mathbf{L}^{\pm} = \left(\mathbf{1} \mp \mathbf{\Lambda}^{\pm}\frac{\Delta t}{\delta x}\right)\mathbf{P}^{-1}\mathbf{G}^{\pm} \tag{30}$$

and the flux limiting matrices as:

$$\mathbf{\Psi}^{\pm}_{i+(1/2)} = \begin{pmatrix} \Psi\left(\frac{(\mathbf{L}^{\pm})^1_{i+(1/2)\pm 1}}{(\mathbf{L}^{\pm})^1_{i+(1/2)}}\right) & 0 & 0 \\ 0 & \Psi\left(\frac{(\mathbf{L}^{\pm})^2_{i+(1/2)\pm 1}}{(\mathbf{L}^{\pm})^2_{i+(1/2)}}\right) & 0 \\ 0 & 0 & \Psi\left(\frac{(\mathbf{L}^{\pm})^3_{i+(1/2)\pm 1}}{(\mathbf{L}^{\pm})^3_{i+(1/2)}}\right) \end{pmatrix} \tag{31}$$

where $(\mathbf{L}^{\pm})^k$ is the k component of the vector $\mathbf{L}^{\pm}$ and Ψ is the flux limiter function. A number of particular flux limiter functions have been defined in the literature (Hirsch 1990).

In this paper we will use the *Superbee* flux limiter:

$$\Psi(r) = \max[0, \min(1, 2r), \min(2, r)] \tag{32}$$

Then, the second order in space and time TVD scheme is written as (Burguete et al. 2007b):

$$\mathbf{U}_i^a = \mathbf{U}_i^n + \Delta t \left\{ \left(\mathbf{G}^+ - \nu \frac{\delta \mathbf{U}}{\delta x} \right)_{i-(1/2)}^n + \left(\mathbf{G}^- + \nu \frac{\delta \mathbf{U}}{\delta x} \right)_{i+(1/2)}^n - \frac{\mathbf{D}_{i+(1/2)}^{n+\theta} - \mathbf{D}_{i-(1/2)}^{n+\theta}}{\delta x} + \right.$$

$$\left. + \frac{1}{2} \left[\left(\mathbf{P} \mathbf{\Psi}^+ \mathbf{L}^+ \right)_{i-(1/2)}^n - \left(\mathbf{P} \mathbf{\Psi}^+ \mathbf{L}^+ \right)_{i-(3/2)}^n + \left(\mathbf{P} \mathbf{\Psi}^- \mathbf{L}^- \right)_{i+(1/2)}^n - \left(\mathbf{P} \mathbf{\Psi}^- \mathbf{L}^- \right)_{i+(3/2)}^n \right] \right\} \tag{33}$$

Second step: infiltration

In a second step, the contribution of the infiltration term is incorporated. Since infiltration is produced at the flow layer in contact with the porous bed (characterized by null velocity in viscous flows), there is no loss of momentum. In order to avoid numerical errors in the form of negative water volumes:

$$\Delta \alpha_i^a = \min(A,\, \Delta t P i)_i^a, \qquad \begin{pmatrix} A \\ Q \\ As \\ \alpha \\ \phi \end{pmatrix}_i^b = \begin{pmatrix} A \\ Q \\ As \\ \alpha \\ \phi \end{pmatrix}_i^a + \Delta \alpha_i^a \begin{pmatrix} -1 \\ 0 \\ -s \\ 1 \\ s \end{pmatrix}_i^a \tag{34}$$

Exact conservation of water volume and solute mass (to the limit of machine accuracy) is produced in this step, since the following equation holds:

$$A_i^b + \alpha_i^b = A_i^a + \alpha_i^a, \quad (As)_i^b + \phi_i^b = (As)_i^a + \phi_i^a \tag{35}$$

Third step: source terms

In the third step, as mentioned in the context of (24), an implicit discretization of the source terms is applied. Taking into account that only the momentum equation contains source terms, the mass conservation and the solute transport equations are trivial in this step :

$$A_i^c = A_i^b, \quad (As)_i^c = (As)_i^b \tag{36}$$

The friction laws considered are singular, tending to infinity for small values of the water depth, which can introduce numerical instabilities in transient calculations. A threshold value for the depth H_{min} will be used in order to avoid those situations. Below that value, the discharge will be set to zero. We use:

- $H_{min} = 0.01m$ for the Manning friction model.
- $H_{min} = l$ for the power law velocity model.

otherwise, a friction factor $r = r(A) = S_f/(|Q|Q)$ depending only of A is defined for the considered friction models, leading to a simple second order equation for the water discharge. Therefore, discharge is evaluated according to:

$$Q_i^c = \begin{cases} 0; & (H_i^c \leq H_{min}) \\ Q_i^b + g\theta\Delta t\{[A(S_0 - r|Q|Q)]_i^c - [A(S_0 - r|Q|Q)]_i^b\}; & (H_i^c > H_{min}) \end{cases} \tag{37}$$

Fourth step: boundary conditions

Inlet and outlet

A correct numerical model for unsteady flow problems must be based not only on a numerical scheme with the required properties but also on an adequate procedure to discretize the boundary conditions. The theory of characteristics provides clear indications about the number of necessary external boundary conditions to define a well posed problem (Hirsch 1990).

In furrow irrigation, where the water flow is always subcritical, both a physical and a numerical boundary condition at the inlet and at the outlet are necessary. The most usual physical boundary condition at the inlet is a discharge hydrograph $Q_{in} = Q_{in}(t)$. At the outlet, it is common practice to use a rating curve of the type $Q_{out} = Q_{out}(H_{out})$. A closed outlet can be considered a particular case with $Q_{out} = 0$. For solute transport, a physical boundary condition at the inlet, usually a concentration input $s_{in}(t)$, and a numerical boundary condition at the outlet are required.

The method of global mass conservation (Burguete et al. 2002; Burguete et al. 2006) is based on enforcing the integral form of the mass conservation extended to all the computational domain in combination with a conservative scheme for the interior points to generate the numerical boundary condition. In order to ensure the global mass conservation of the scheme, the numerically generated volume variation must be combined with the desired volume variation and therefore the following corrections must be enforced over the wetted cross section at the inlet:

$$A_1^{n+1} = A_1^c + \frac{\int_{t^n}^{t^{n+1}} Q_{in}(t)dt - \Delta t Q_1^n}{\delta x}, \quad (As)_1^{n+1} = (As)_1^c + \frac{\int_{t^n}^{t^{n+1}} Q_{in}(t)s_{in}(t)dt - \Delta t (Qs)_1^n}{\delta x} \tag{38}$$

In order to ensure the correct formulation of the boundary we must enforce subcritical flow at the inlet in the following form:

$$Q_1^{n+1} = \min[Q_{in}(t^{n+1}),\ A_1^{n+1}c_1^{n+1})] \tag{39}$$

At the outlet, an exact estimation of the outflowing mass is impossible when using a rating curve as boundary condition. Hence the following approximations are used:

$$Q_N^{n+1} = \min[Q_{out}(H_N^{n+1}),\ A_N^{n+1}c_N^{n+1}], \quad A_N^{n+1} = A_N^c, \quad (As)_N^{n+1} = (As)_N^c \tag{40}$$

Furrow junctions

We will concentrate on furrow junctions of the "T" type, that is, involving only a main furrow and a perpendicular secondary furrow as in Figure 4. In this way, the momentum addition from the tributary furrow is in the normal direction to the main flow and viceversa.

The main hypothesis used to solve at the junction area is that the m main furrow grid cells involved at the junction (from j to $j+m$) as well as the secondary furrow grid cell involved (k) share a unique water surface level and a unique value of solute concentration. The total volume of water $V^c_{junction}$ and mass of solute $M^c_{junction}$at the junction cells are therefore:

$$V^c_{junction} = A^c_k \delta x_k + \sum_{i=j}^{j+m} A^c_i \delta x_i, \quad M^c_{junction} = (As)^c_k \delta x_k + \sum_{i=j}^{j+m} (As)^c_i \delta x_i, \tag{41}$$

By requiring the conservation of water volume and the uniform surface water level z_s^{n+1}, a second order equation for this variable can be written:

$$V^{n+1}_{junction} = \{(B_0)_k + S_k[(z_s)^{n+1}_k - (z_b)_k]\}[(z_s)^{n+1}_k - (z_b)_k]\delta x_k +$$

$$+ \sum_{i=j}^{j+m} \{(B_0)_i + S_i[(z_s)^{n+1}_i - (z_b)_i]\}[(z_s)^{n+1}_i - (z_b)_i]\delta x_i = V^c_{junction} \tag{42}$$

this formulation immediately leads to the values of A_i^{n+1} and A_k^{n+1}. On the other hand, the requirements of solute mass conservation and uniform concentration at the junction result in:

$$s_i^{n+1} = s_k^{n+1} = \frac{M^c_{junction}}{V^c_{junction}}, \ \forall i \in [j, j+m] \tag{43}$$

Finally, momentum interchanges at the junction must be considered. We will assume that velocity is uniform in a cell, so that the momentum exchange is proportional to mass exchange. In fact, the furrow supplying mass to the confluence loses an amount of momentum in its longitudinal direction which is proportional to its loss of mass. However, since the confluence is perpendicular, the furrow supplies momentum in perpendicular fashion, with

no component in the longitudinal direction of the receiving furrow. Taking this effect into account, the following correction over the discharges at the junction grid cells is performed:

$$Q_i^{n+1} = \begin{cases} Q_i^c; & (A_i^c \leq A_i^{n+1}) \\ Q_i^c \frac{A_i^{n+1}}{A_i^c}; & (A_i^c > A_i^{n+1}) \end{cases}, \quad Q_k^{n+1} = \begin{cases} Q_k^c; & (A_k^c \leq A_k^{n+1}) \\ Q_k^c \frac{A_k^{n+1}}{A_k^c}; & (A_k^c > A_k^{n+1}) \end{cases} \tag{44}$$

TEST CASES AND APPLICATIONS

Test I: ideal dambreak with solute discontinuity

The ideal dambreak problem is one of the classical examples used as test case for unsteady shallow water flow simulations. The reason is that for flat and frictionless bottom, rectangular cross section and no diffusion, the problem defined by zero initial velocity and initial discontinuities in the water depth and solute concentration has an exact solution (Stoker 1957).

A rectangular channel $200m$ long and $1m$ wide has been considered with an initial depth ratio $1m : 0.1m$ and with an initial discontinuity in the concentration of $1kg/m^3 : 0kg/m^3$ in the same location as the depth jump. A grid spacing of $\delta x = 2m$, $CFL = 0.9$ and $t = 20s$ was used for all simulations.

The plots in Figure 5 show the numerical solution for the water depth from the numerical scheme described in this work and for the classical McCormack scheme (García-Navarro and Savirón 1992) versus the exact solution for $t = 20s$. The numerical scheme used in this research clearly shows better performance than classical MacCormack.

Figure 6 shows the results for the solute concentration provided by the 2nd order TVD scheme using the discretization described in this work and the separate discretization (see (Burguete et al. 2007b) for different discretizations of the solute transport equation with this scheme), and the classical McCormack scheme. The proposed scheme yields best results when used in conjunction with the proposed discretization.

Test II: closed furrows with a confluence

In this section, the performance of the proposed numerical scheme is assessed for different treatments of the boundary conditions in a set of two furrows closed in their downstream ends and arranged in a "T" confluence. Figure 7 presents the geometry of the test case. Furrows have a trapezoidal section with dimensions $B_0 = 0.20m$, $S = 1$, $S_0 = 0$ and a depth of $0.4m$. Roughness is modelled using Gauckler-Manning equation (18) with $n = 0.03sm^{-1/3}$, solute diffusion follows Rutherford equation (21), and infiltration follows equation (16), with $K = 0.0015ms^{-a}$ and $a = 0.3$. These parameters are characteristic of a low infiltration clay soil. The furrow spacing, D, is $1m$. A constant inflow $Q_{in} = 0.01m^3/s$ is introduced in the domain with a solute concentration of $s_{in} = 1kg/m^3$. Although the problem does not have an analytical solution, the total water volume and solute mass follow:

$$V = Q_{in}t, \quad M = Q_{in}s_{in}t \tag{45}$$

These volumes and masses can be compared with the numerical results, which are computed as:

$$V^n = \sum_{i=1}^{N}(A+\alpha)_i^n \delta x, \quad M^n = \sum_{i=1}^{N}(As+\phi)_i^n \delta x \tag{46}$$

The respective conservation errors can be determined as:

$$E_V = 100\frac{V^n - V}{V}\%, \quad E_M = 100\frac{M^n - M}{M}\% \tag{47}$$

Figure 8 presents the longitudinal profiles of H as a function of the distance to the upstream inlet point, using the proposed numerical scheme and treatments of the boundary conditions and the confluence for (a) $t = 900s$ and (b) $t = 1500s$.

Table 1 presents a comparison of the mass errors at time $t = 1500s$ with the proposed treatments for the boundary conditions (global mass conservation) and the confluence (conservative junction). Results are also provided for other treatments of the boundary condi-

tions (local mass conservation (Jin and Fread 1997)) and a simple treatment of the confluence based on equalling the free water surface level and the solute concentration at the receiving furrow to the supplying furrow at the confluence. Different combinations of treatments result in large errors, while the combination of proposed treatments reduces the conservation errors to machine accuracy.

Test III: Confluence with experimental measurements

Qu (2005) and Ramamurthy et al. (2007) reported an experimental and numerical analysis of the flows resulting from a confluence in a laboratory channel. These papers include a detail flow analysis and simulations performed with a 3D numerical model. Since the channel walls were smooth, the Manning roughness model was used, with $n = 0.009 s m^{-1/3}$.

In the practical simulation of a level-furrow system there is a large number of confluences between the conveyance channels and the irrigation furrows. Additionally, the computational mesh required to simulate these problems in reasonable time is often coarse. As a consequence, the computational time devoted to each confluence is limited, and the confluence should be simulated as just one cell in the conveyance channel and another cell in the irrigation furrow.

Test III was performed to assess if - despite its crude approach - the proposed two-cell confluence can produce a reasonable approximation of the flow partition. Figure 9 presents a scheme of the experimental device and the simulation mesh. A mesh with $\delta x = 0.61 m$, in the range of typical furrow simulations, was designed. The mesh uses 14 cells for the main furrow and 4 for the secondary furrow, with the confluence involving just one cell in each furrow.

The paper by Qu (2005) reports measurements of discharge, flow depth and velocity for five different flow conditions obtained through modifications of the weirs installed at the downstream end of each furrow. However, the author did not report on the settings (elevations) of the regulating weirs. In order to overcome this difficulty, a critical flow law was implemented at the downstream end of each furrow using a range of weir settings.

The weir setting minimizing the error between measured and simulated measurements was adopted as representative of the experimental conditions. Let h_m^e be the flow depth, with $\overline{h_m^e}$ the average value and n_m^e the number of experimental measurements in the main furrow; h_m^s will be the simulated flow depth at the main furrow. In the secondary furrow these magnitudes will be denoted as h_s^e, $\overline{h_s^e}$, n_s^e and h_s^s, respectively. Additionally, Q_{in} will be the inflow discharge, Q_s^e and Q_s^s will be the experimental and simulated discharge at the secondary furrow, respectively. In these conditions, the error can be defined as:

$$E = \frac{|Q_s^e - Q_s^s|}{Q_{in}} + \frac{1}{\overline{h_m^e}}\sqrt{\frac{\sum_{i=1}^{n_m^e}[(h_m^e)_i - (h_m^s)_i]^2}{n_m^e - 1}} + \frac{1}{\overline{h_s^e}}\sqrt{\frac{\sum_{i=1}^{n_s^e}[(h_s^e)_i - (h_s^s)_i]^2}{n_s^e - 1}} \tag{48}$$

The model will be considered valid if under conditions of minimum error it can reproduce the experimental measurements in a reasonable fashion.

Table 2 presents the discharges measured at the inflow and at the secondary furrow for the five experimental flow conditions, together with the optimum weir settings resulting in minimum error according to (48). Figure 10 presents maps of the errors corresponding to the main and secondary weir settings in the five reported flow conditions. It can be concluded that the weir settings could be estimated in an accurate way. Figure 11 presents a scatter plot of experimental vs. optimum simulated discharge at the secondary channel for the different flow conditions. All five points are distributed along the $1:1$ line, providing an additional indication of the accuracy in the estimation of the weir settings. Finally, Figure 12 presents the longitudinal profiles for flow depth (measured and simulated). The agreement between both sources of data suggests that the proposed simple method for hydraulic computations in confluences is accurate enough to be used in the simulation of a level furrow system.

CONCLUSIONS

A mathematical model including shallow water flow and solute transport has been presented and solved using a second order TVD scheme. The model is adapted to furrow

fertigation and implements an infiltration equation that automatically adjusts to variations in the wetted perimeter, a roughness equation based on an absolute roughness parameter, and an equation for the estimation of the longitudinal diffusion parameter. The parameterization problem is therefore reduced to estimating infiltration in reference conditions, and estimating a physically based roughness parameter that will result in a flow-dependent roughness. The model also incorporates a specific treatment of the boundary conditions formulated to ensure global mass conservation at machine accuracy.

In order to extend the model to furrow networks, a simple and computationally efficient approach to the junction conditions, considered as internal boundaries, has been proposed. Three numerical tests have been used to assess the shock-capturing model properties for both water level and solute concentration front advance, and to evaluate the performance of the treatment of boundary conditions and junctions. The results of these tests have confirmed the adequacy of the model to address the problems of unsteady flows with solute transport in single channels and junctions in channels. In a companion paper the model is calibrated and validated using *ad hoc* furrow fertigation experiments, and is applied to the simulation of level furrow systems.

NOTATION

A = cross-sectional wetted area;

a = Kostiakov infiltration exponent;

B = cross section top width;

B_0 = cross section base width;

c = velocity of the infinitesimal waves;

D = distance between furrows;

$\mathbf{D}$ = diffusion vector;

400 E_M = error of solute mass conservation;

401 E_V = error of water volume conservation;

402 $\mathbf{F}$ = conservative flux vector;

403 g = gravitational constant;

404 H = cross-sectional maximum water depth;

405 h = water depth;

406 H_{min} = minimum depth to allow water flowing;

407 $\mathbf{I}$ = infiltration vector;

408 i = infiltration rate;

409 I_1, I_2 = pressure force integrals;

410 $\mathbf{J}$ = conservative flux Jacobian,

411 K = Kostiakov infiltration parameter;

412 K_x = diffusion coefficient;

413 L = weir setting (elevation over the furrow base);

414 $\mathbf{L}$ = second order vector;

415 l = characteristic roughness length;

416 M = solute mass;

417 n = Gauckler-Manning roughness coefficient;

418 P = cross-sectional wetted perimeter;

419 $\mathbf{P}$ = Jacobian eigenvectors matrix;

Q = discharge;

Q_{in} = inlet hydrograph discharge;

Q_{out} = outlet rating curve of discharge;

r = friction factor;

S = furrow wall slope;

s = cross-sectional average solute concentration;

S_0 = longitudinal bottom slope;

$\mathbf{S}^c$ = conservative source term vector;

S_f = longitudinal friction slope;

s_{in} = inlet solute concentration input;

$\mathbf{S}^{nc}$ = non-conservative source term;

t = time;

$\mathbf{U}$ = conserved variable vector;

u = cross-sectional averaged velocity;

V = water volume;

v_x = longitudinal component of the velocity at any point of the cross section;

w = cross section width;

x = longitudinal coordinate;

y = transversal coordinate;

Z = cumulative infiltration length;

z = vertical coordinate;

z' = vertical distance to bed level;

z'' = vertical distance over the lowest point in the cross section;

z_b = level of the lowest point in the cross section;

z_s = water surface level;

α = infiltrated cross section;

Δ = temporal finite increment;

δ = spatial finite increment;

ϵ = friction coefficient;

$\mathbf{\Lambda}$ = eigenvalues diagonal matrix;

λ_i = Jacobian eigenvalues;

ϕ = solute mass infiltrated per unit length of the furrow; and

τ = opportunity time.

References

Abbasi, F., Feyen, J., Roth, R. L., Sheedy, M., and van Genuchten, M. T. (2003a). "Water flow and solute transport in furrow-irrigated fields." *Irrig. Sci.*, 22, 57–65.

Abbasi, F., Simunek, J., van Genuchten, M. T., Feyen, J., Adamsen, F. J., Hunsaker, D. J., Strelkoff, T., and Shouse, P. J. (2003b). "Overland water flow and solute transport: model development and field-data analysis." *ASCE J. Irrig. and Drainage Eng.*, 129(2), 71–81.

Adamsen, F. J., Hunsaker, D. J., and Perea, H. (2005). "Border strip fertigation: effect of injection strategies on the distribution of bromide." *Trans. of the ASAE*, 48(2), 529–540.

Bear, J. (1972). *Dynamics of fluids in porous media*. Elsevier Science, New York, USA.

462 Boldt, A. L., Watts, D. G., Eisenhauer, D. E., and Schepers, J. S. (1994). "Simulation of
463 water applied nitrogen distribution under surge irrigation." *Trans. of the ASAE*, 37(4),
464 1157–1165.
465 Burguete, J. and García-Navarro, P. (2004). "Implicit schemes with large time steps for non-
466 linear equations: application to river flow hydraulics." *Int. J. for Numerical Methods in*
467 *Fluids*, 46(6), 607–636.
468 Burguete, J., García-Navarro, P., and Aliod, R. (2002). "Numerical simulation of runoff from
469 extreme rainfall events in a mountain water cachtment." *Natural Hazards in Earth System*
470 *Sci.*, 2, 1–9.
471 Burguete, J., García-Navarro, P., and Murillo, J. (2006). "Numerical boundary conditions
472 for globally mass conservative methods to solve the shallow-water equations and applied
473 to river flow." *Int. J. for Numerical Methods in Fluids*, 51(6), 585–615.
474 Burguete, J., García-Navarro, P., and Murillo, J. (2007a). "Friction term discretization and
475 limitation to preserve stability and conservation in the 1d shallow-water model: application
476 to unsteady irrigation and river flow." *Int. J. for Numerical Methods in Fluids*, in press.
477 Burguete, J., García-Navarro, P., and Murillo, J. (2007b). "Preserving bounded and con-
478 servative solutions of transport in 1d shallow-water flow with upwind numerical schemes:
479 application to fertigation and solute transport in rivers." *Int. J. for Numerical Methods*
480 *in Fluids*, in press.
481 Burguete, J., García-Navarro, P., Murillo, J., and García-Palacín, I. (2007c). "Analysis of
482 the friction term in the one-dimensional shallow water model." *ASCE J. Hydraulic Eng.*,
483 133(9), 1048–1063.
484 García-Navarro, P., Playán, E., and Zapata, N. (2000). "Solute transport modeling in over-
485 land flow applied to fertigation." *ASCE J. Irrig. and Drainage Eng.*, 126(1), 33–41.
486 García-Navarro, P., Sánchez, A., Clavero, N., and Playán, E. (2004). "A simulation model
487 for level furrows II: description, validation and application." *ASCE J. Irrig. and Drainage*
488 *Eng.*, 130(2), 113–121.

García-Navarro, P. and Savirón, J. M. (1992). "McCormack's method for the numerical simulation of one-dimensional discontinuous unsteady open channel flow." *J. Hydraulic Res.*, 30(1), 95–105.

Gauckler, P. G. (1867). "Études théoriques et practiques sur l'écoulement et le mouvement des eaux." Comptes Rendues de l'Académie des Sciences, Paris.

Hirsch, C. (1990). *Computational methods for inviscid and viscous flows: Numerical computation of internal and external flows*. John Wiley & Sons, New York.

Jin, M. and Fread, D. L. (1997). "Dynamic flood routing with explicit and implicit numerical solution schemes." *ASCE J. Hydraulic Eng.*, 123(3), 166–173.

Maïkaka, M. (2004). "Modelos numéricos unidimensionales en riego por superficie," PhD thesis, University of Zaragoza.

Manning, R. (1890). "On the flow of water in open channels and pipes." Institution of Civil Engineers of Ireland.

Playán, E. and Faci, J. M. (1997). "Border fertigation: field experiments and a simple model." *Irrig. Sci.*, 17, 163–171.

Playán, E., Rodríguez, J. A., and García-Navarro, P. (2004). "Simulation model for level furrows. I: analysis of field experiments." *ASCE J. Irrig. and Drainage Eng.*, 130(2), 106–112.

Qu, J. (2005). "Three-dimensional turbulence modeling for free surface flows," PhD thesis, Concordia University.

Ramamurthy, A. S., Qu, J., and Vo, D. (2007). "Numerical and experimental study of dividing open-channel flows." *ASCE J. Hydraulic Eng.*, 133(10), 1135–1144.

Rutherford, J. C. (1994). *River mixing*. John Wiley & Sons.

Sabillón, G. N. and Merkley, G. P. (2004). "Fertigation guidelines for furrow irrigation." *Spanish Journal of Agricultural Research*, 2, 576–587.

Simunek, J., Sejna, M., and van Genuchten, M. T. (1998). "The HYDRUS-1D software package for simulating the movement of water, heat and multiple solutes in variably saturated

porous media, version 2.0." United States Salinity Laboratory, USDA-ARS, Riverside, California. USA.

Stoker, J. J. (1957). *Water waves*. Interscience, New York.

Strelkoff, T. S., Clemmens, A. J., and Perea-Estrada, H. (2006). "Calculation of non-reactive chemical distribution in surface fertigation." *Agric. Water Mgmt.*, 86(1–2), 93–101.

Walker, W. R. and Skogerboe, G. V. (1987). *Surface irrigation. Theory and practice*. Prentice-Hall, Inc., Englewood Cliffs, New Jersey.

Zerihun, D., Furman, A., Warrick, A. W., and Sanchez, C. A. (2005a). "Coupled surface-subsurface solute transport model for irrigation borders and basins I: model development." *ASCE J. Irrig. and Drainage Eng.*, 131(5), 396–406.

Zerihun, D., Sanchez, C. A., Furman, A., and Warrick, A. W. (2005b). "Coupled surface-subsurface solute transport model for irrigation borders and basins II: model evaluation." *ASCE J. Irrig. and Drainage Eng.*, 131(5), 407–419.

List of Tables

List of Figures

List of Tables

Table 1. Errors in water volume and solute mass conservation in Test II at time $t = 1500s$ as solved with the proposed treatments for the boundary conditions (global mass conservation, GC) and the confluence (conservative junction, CJ). Results are also provided for other treatments of the boundary conditions (local mass conservation LC) and a simple treatment of the confluence (SC).

Numerical treatments	$E_V(\%)$	$E_M(\%)$
LC+SJ	46.6	46.5
GC+SJ	45.9	45.9
LC+CJ	0.37	0.28
GC+CJ	$-2.0 \cdot 10^{-15}$	$-2.0 \cdot 10^{-15}$

Table 2. Discharges measured at the inflow and at the secondary furrow for the five experimental flow conditions, together with the optimum weir settings (elevation over the furrow base, L) resulting in minimum simulation error.

Case	Q (m^3/s)	Q (m^3/s)	L (m)	L (m)	Error
	inlet	secondary	main	secondary	
IIIa	0.047	0.007	0.110	0.156	0.034
IIIb	0.046	0.014	0.098	0.108	0.031
IIIc	0.046	0.019	0.104	0.092	0.067
IIId	0.047	0.032	0.145	0.088	0.082
IIIe	0.046	0.038	0.180	0.102	0.078

List of Figures

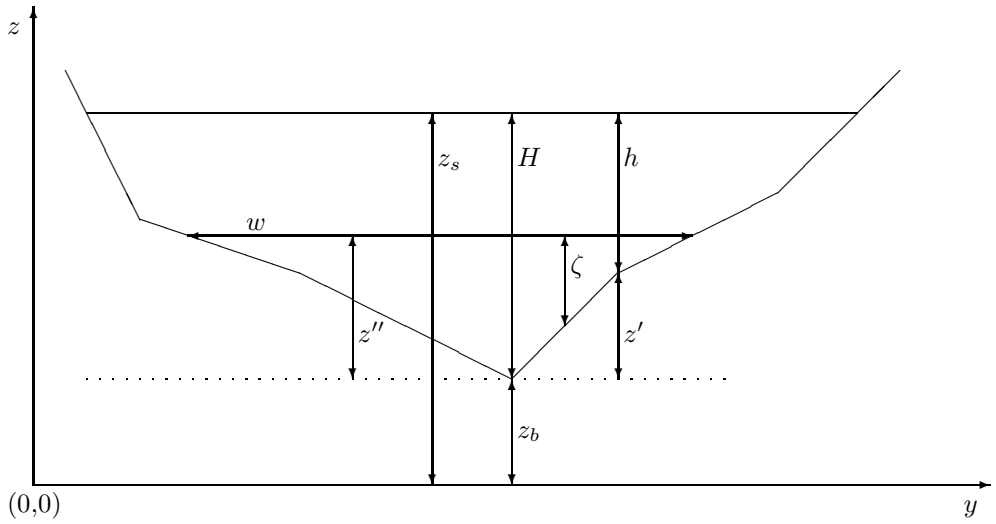

Figure 1. Coordinate system in a cross section.

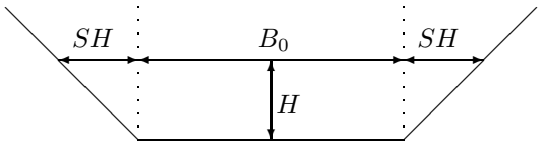

Figure 2. Trapezoidal furrow geometry

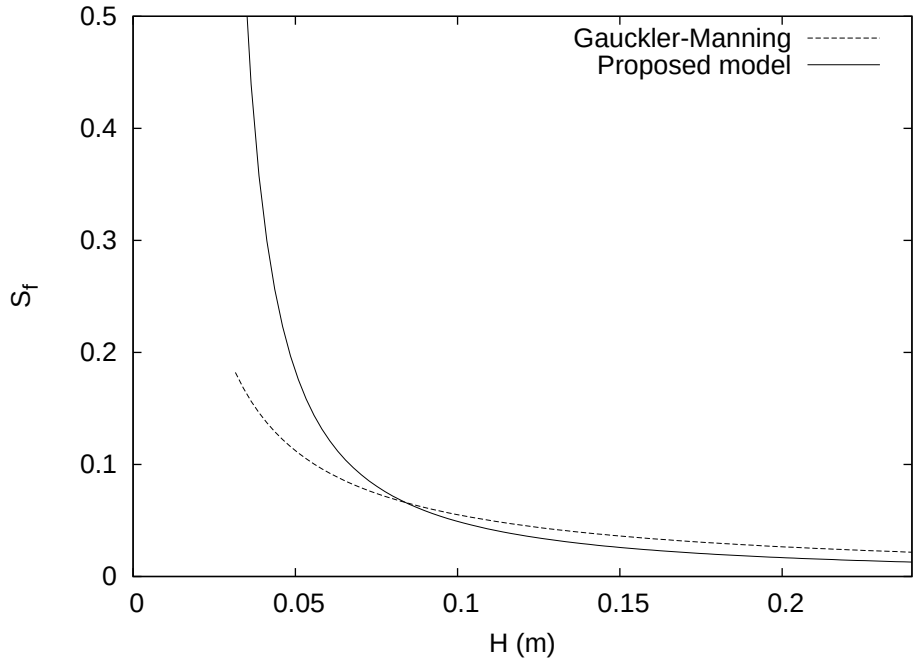

Figure 3. S_f **versus** H **for a flow velocity** $U = 1m/s$ **and a typical furrow shape with** $B_0 = 0.14m$**,** $S = 1.22$ **and where** $n = 0.035sm^{-1/3}$**,** $\epsilon = 0.04$**,** $b = 0.25$ **and** $l = 0.02m$**.**

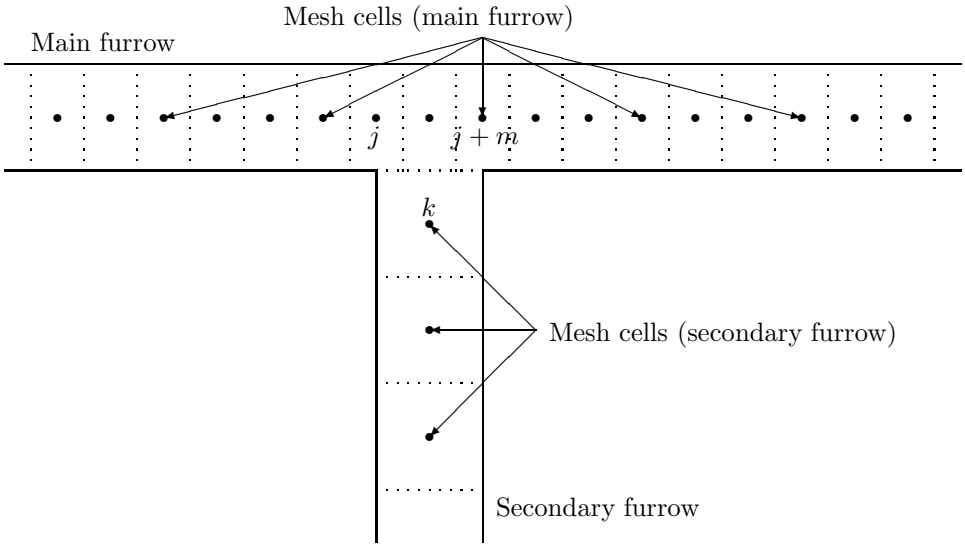

Figure 4. Discretization at a junction. The grid cells j to $j+m$ at the main furrow and the grid cell k at the secondary furrow are involved in the junction.

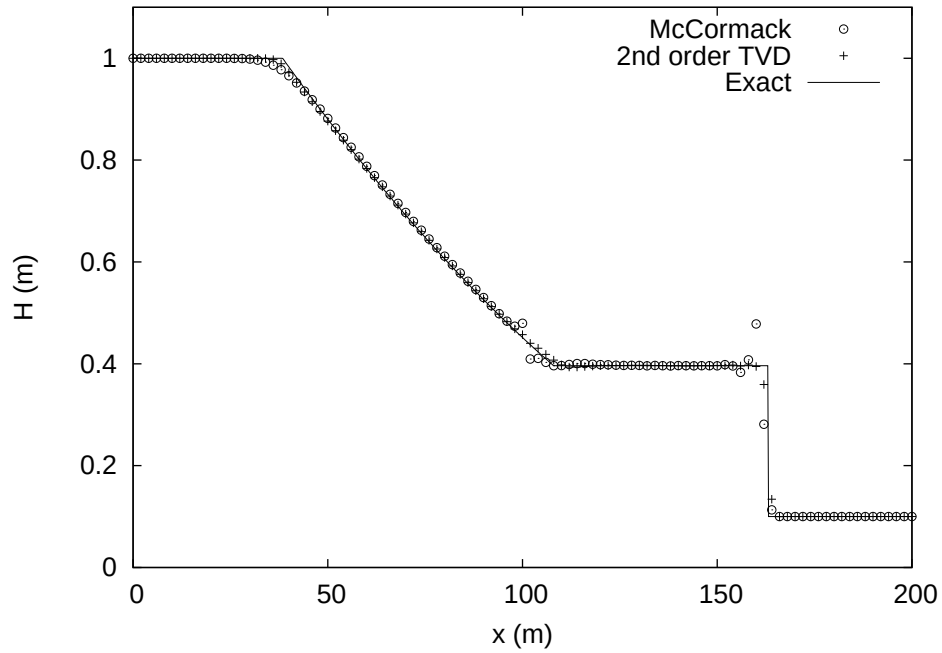

Figure 5. Ideal dambreak depth with McCormack and 2nd order TVD schemes.

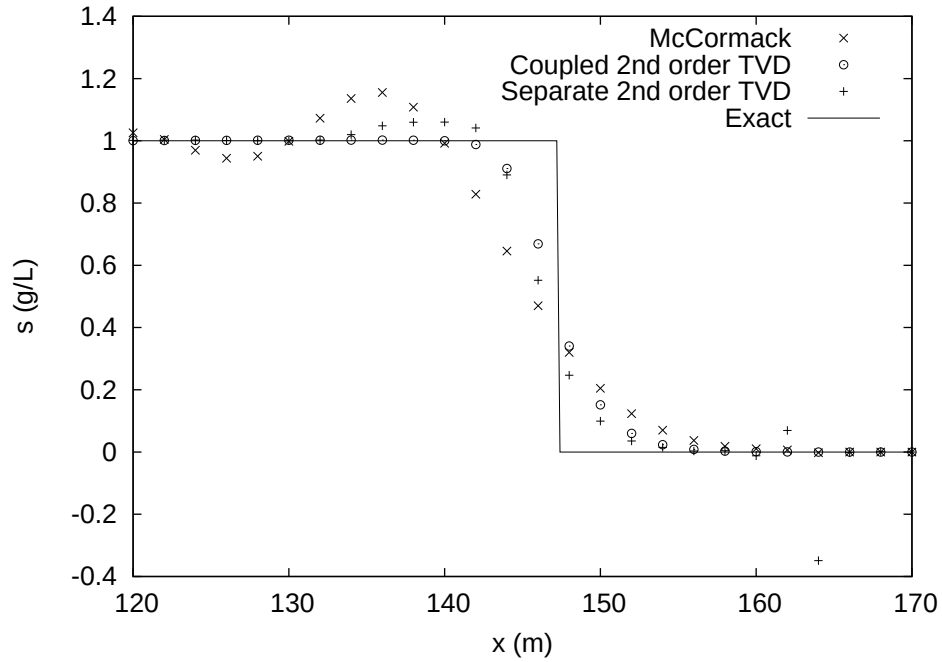

Figure 6. Results of Test I, dambreak with discontinuous concentration, for $t = 20s$ with the MacCormack method, the proposed coupled 2nd order TVD, the separate 2nd order TVD and the exact solution.

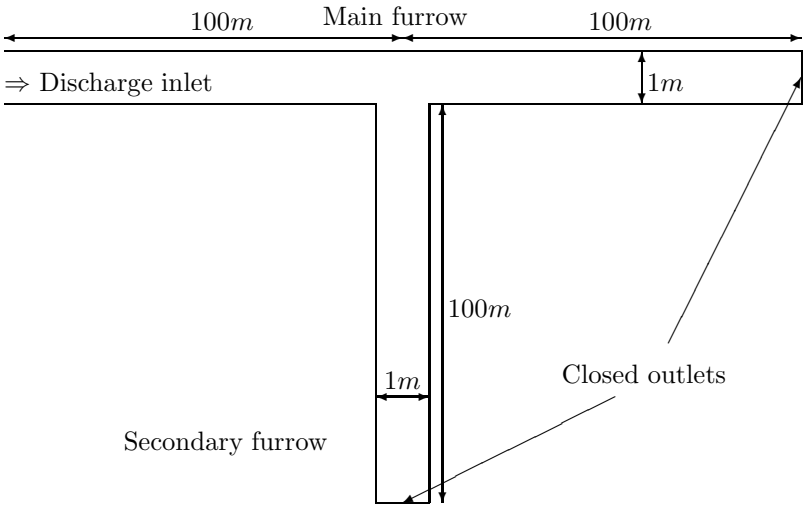

Figure 7. Plan view of the simulated system in Test II.

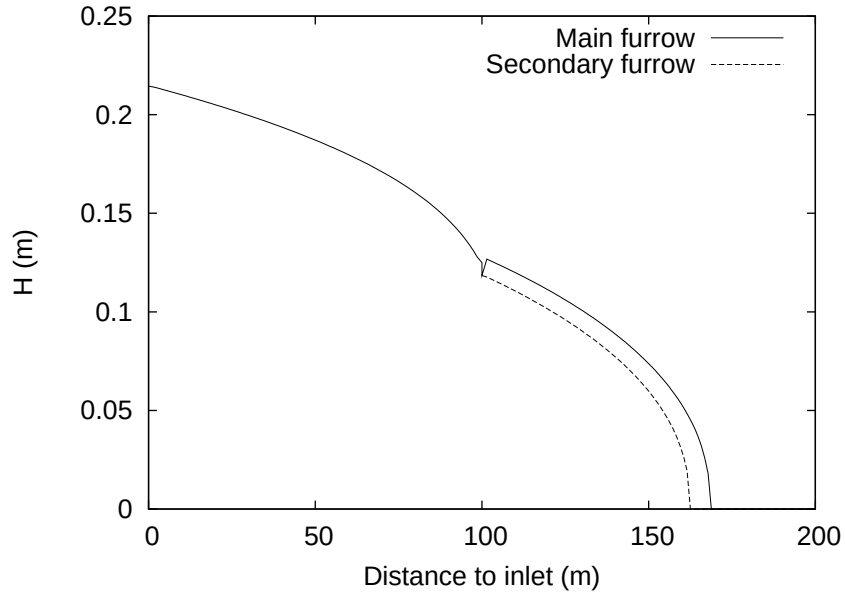

(a)

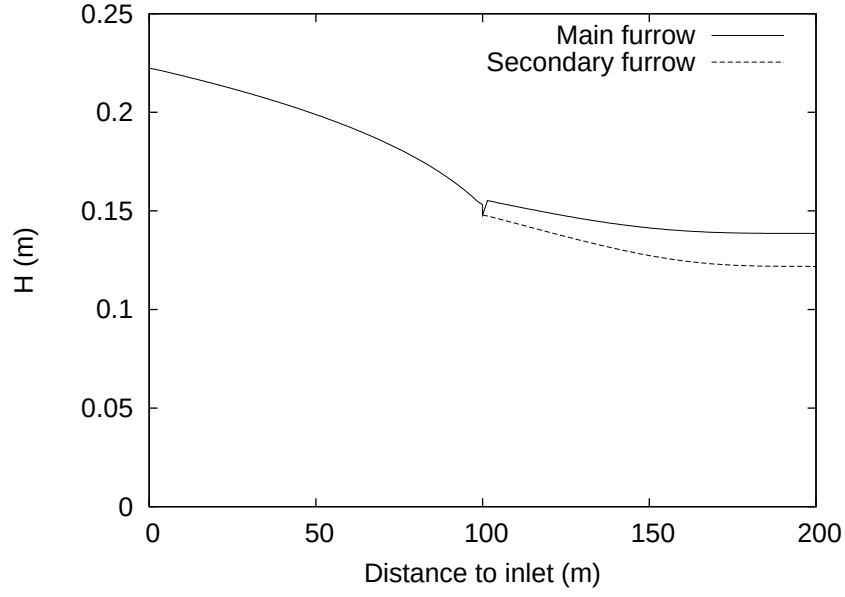

(b)

Figure 8. Longitudinal profiles of flow depth as a function of the distance to the upstream inlet for Test II with the proposed numerical scheme and treatments for (a) $t = 900s$ **and (b)** $t = 1500s$**.**

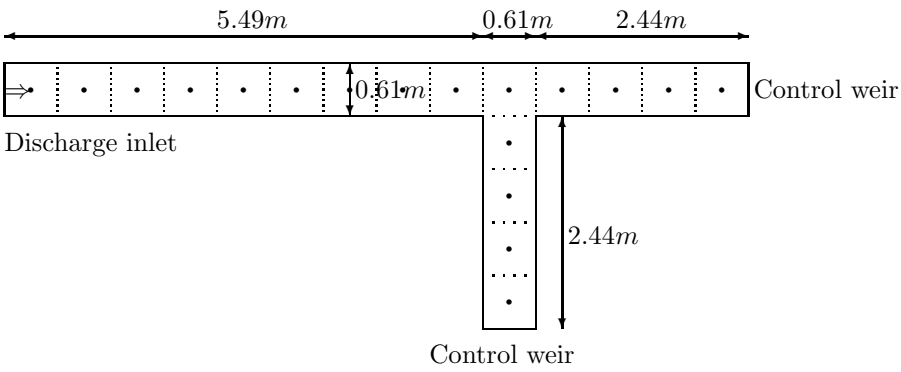

Figure 9. Test III: plan view of the experimental system and scheme of the mesh used for its simulation.

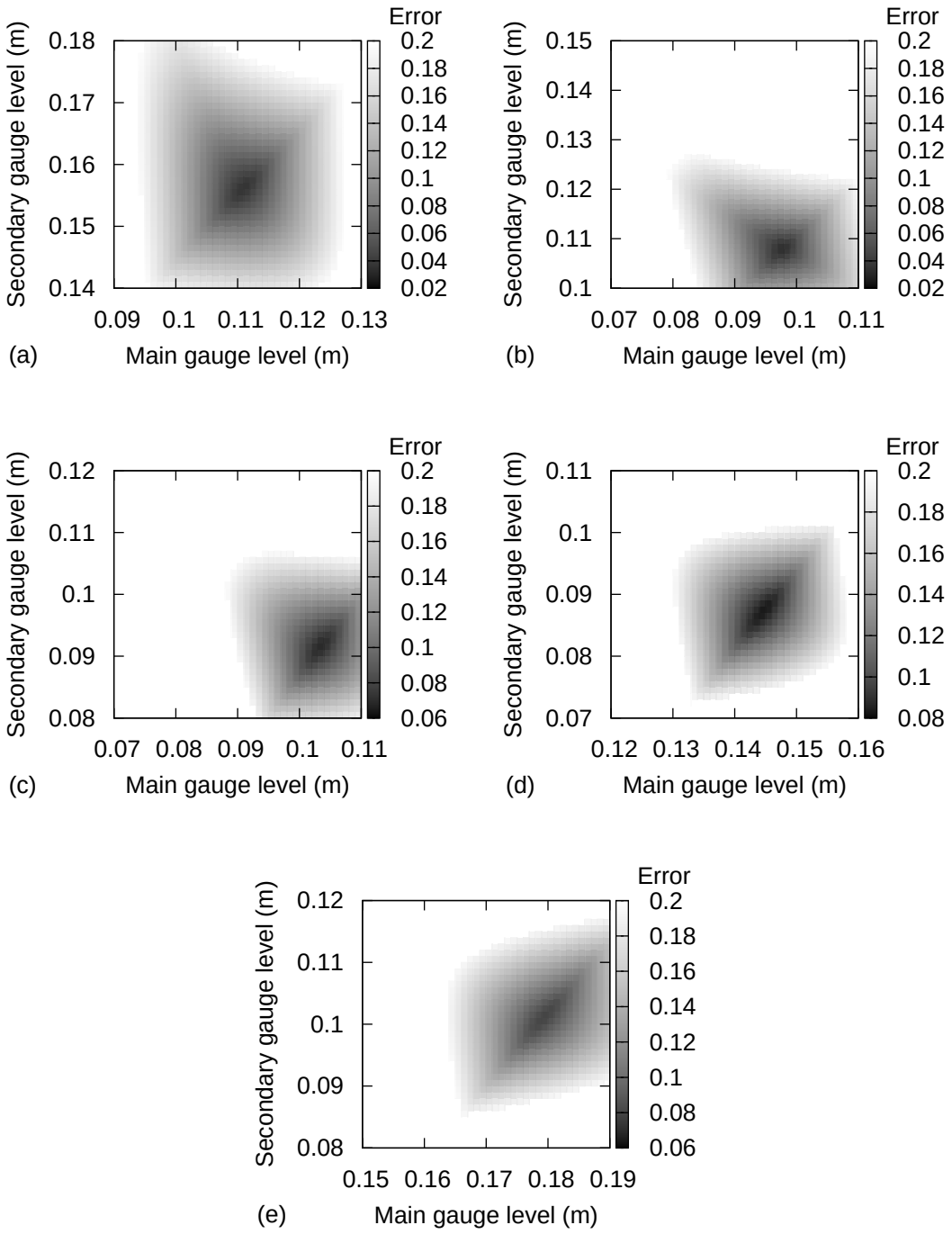

Figure 10. Map of simulation error as a function of the weir settings for the five flow conditions reported in Test III.

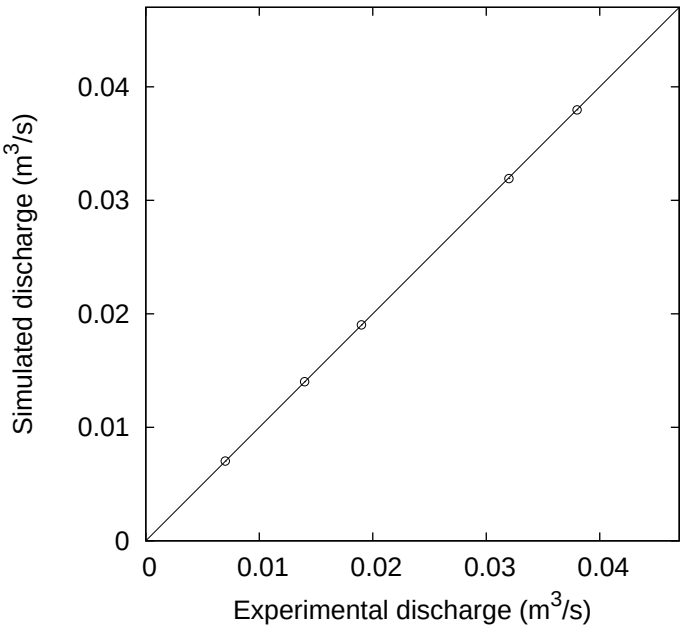

Figure 11. Scatter plot of experimental vs. simulated discharge at the secondary channel for the five flow conditions described in Test III.

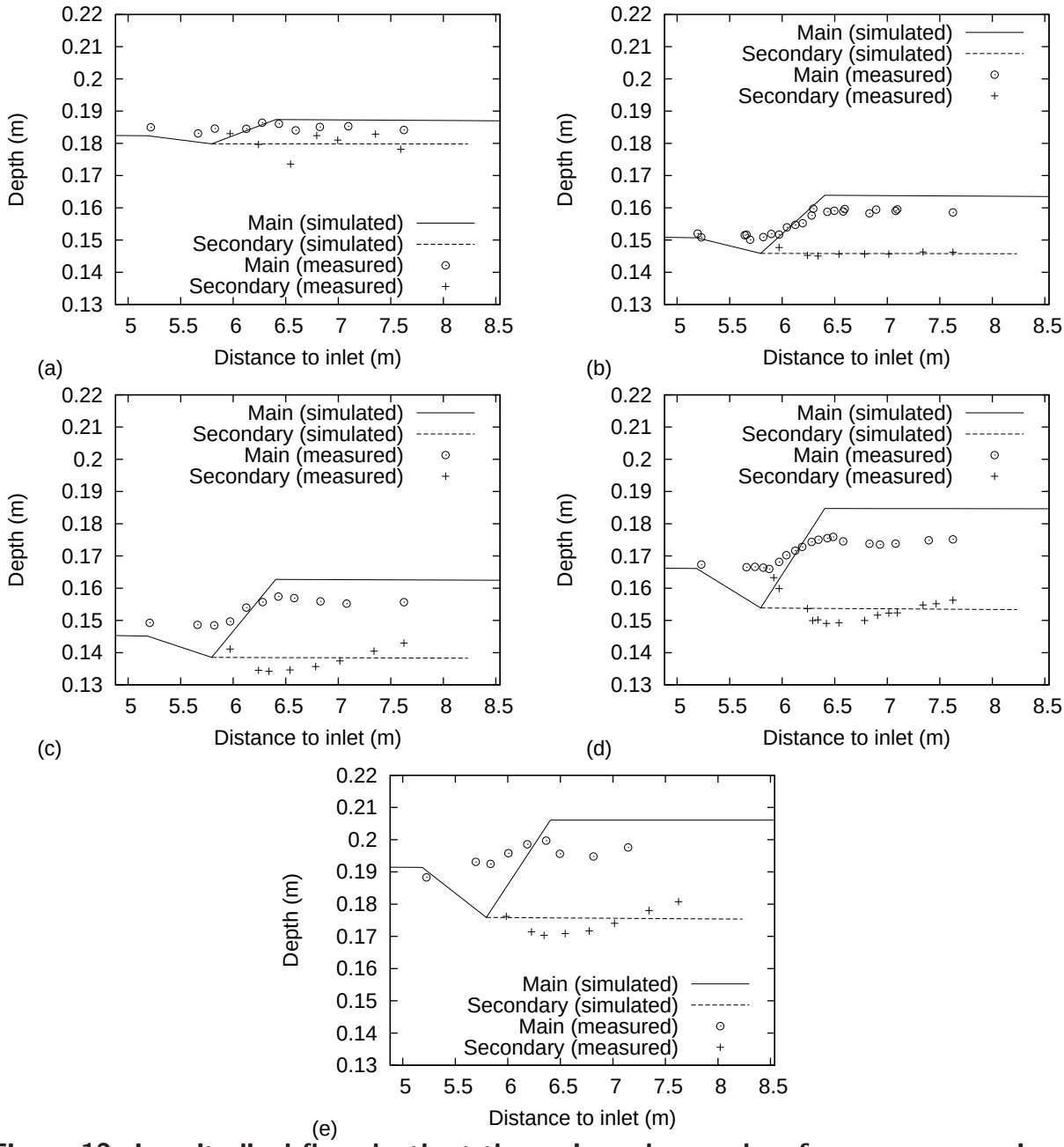

Figure 12. Longitudinal flow depth at the main and secondary furrows, as experimentally observed and simulated, for the five flow conditions described in test III.